# Synthesis, Characterization, and Electronic Structure of Single-Crystal SnS, Sn$_2$S$_3$, and SnS$_2$

Lee A. Burton,[†] Diego Colombara,[‡] Ruben D. Abellon,[§] Ferdinand C. Grozema,[§] Laurence M. Peter,[†] Tom J. Savenije,[§] Gilles Dennler,[⊥] and Aron Walsh*[,†]

[†]Centre for Sustainable Chemical Technologies, Department of Chemistry, University of Bath, Bath, United Kingdom

[‡]Laboratory for Energy Materials, Université du Luxembourg, 41, rue du Brill, L-4422 Belvaux, Luxembourg

[§]Opto-Electronic Materials Section, Department of Chemical Engineering, Faculty of Applied Sciences, Delft University of Technology, Julianalaan 136, 2628 BL Delft, The Netherlands

[⊥]Department Energy and the Environment, IMRA Europe SAS, 220 rue Albert Caquot, BP213, F-06904 Sophia Antipolis Cedex, France

S *Supporting Information*

ABSTRACT: Tin sulfide is being widely investigated as an earth-abundant light harvesting material, but recorded efficiencies for SnS fall far below theoretical limits. We describe the synthesis and characterization of the single-crystal tin sulfides (SnS, SnS$_2$, and Sn$_2$S$_3$) through chemical vapor transport, and combine electronic structure calculations with time-resolved microwave conductivity measurements to shed light on the underlying electrical properties of each material. We show that the coexistence of the Sn(II) and Sn(IV) oxidation states would limit the performance of SnS in photovoltaic devices due to the valence band alignment of the respective phases and the "asymmetry" in the underlying point defect behavior. Furthermore, our results suggest that Sn$_2$S$_3$, in addition to SnS, is a candidate material for low-cost thin-film solar cells.

KEYWORDS: *semiconductor, earth-abundant, photovoltaic, tin sulfide, workfunction*
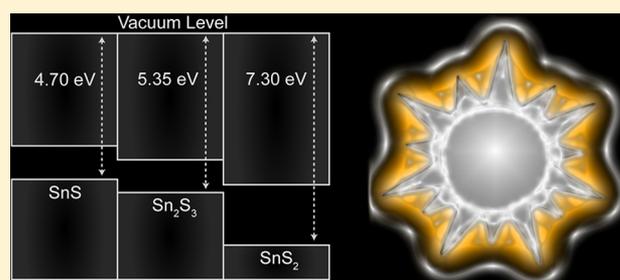
■ INTRODUCTION

In order for photovoltaic (PV) technology to provide a significant fraction of the world's energy demands, devices must be composed of cheap and abundant materials.[1] Tin monosulfide (SnS) is increasingly being investigated as a photoconverter because it is neither scarce, expensive, nor toxic,[2] unlike commercially available cadmium telluride (CdTe) or copper–indium–gallium–diselenide (CIGS).[3] It is also a binary component of the popular copper–zinc–tin–sulfide (CZTS) absorber system.[4]

SnS exhibits almost ideal electronic properties for PV applications, including a higher optical absorption coefficient than CdTe,[5,6] and an effective onset of optical absorption that coincides with the optimum band gap for maximum efficiency according to the Shockley–Queisser limit within the AM 1.5 solar spectrum.[7−11] As a result, a theoretical conversion efficiency of 24% for SnS single-junction devices is predicted from Prince–Loferski diagrams.[8,12−14] SnS also does not require extrinsic doping because of intrinsic p-type conductivity brought about by the formation of tin vacancies.[15] All of this suggests that the application of SnS in thin film photovoltaics could lead to devices with low cost and high market penetration.[16] In practice, however, the highest certified light-to-electricity conversion efficiency of SnS devices is still only

2.0%,[17] despite the first SnS PV device being reported in 1997 with a 0.5% efficiency.[18]

The poor performance of SnS solar cells to date could be related to a number of materials issues including: (i) low quality single phase materials, i.e. single phase SnS with defect and carrier concentrations and/or morphology that is not optimal. (ii) Device architecture, i.e. the commonly used electrical contacts and buffer layer materials are unsuitable for high conversion efficiencies.[19,20] (iii) Mixed phases, i.e., the presence of alternate SnS polytypes, Sn$_2$S$_3$ or SnS$_2$, may be detrimental to the photovoltaic performance.[21,22] The first issue could be avoidable under suitable synthesis conditions,[23−25] and the second could be investigated by varying the materials used as electrical contacts.[19,20] We address the third outstanding issue in this work, investigating the three distinct stoichiometries of tin sulfide and the properties of each.

As a heavier element in Group 14 of the Periodic Table, Sn has two accessible oxidation states: divalent (electronic configuration [Kr]4d^{10}5s^{2}5p^0) and tetravalent (electronic configuration [Kr]4d^{10}5s^{0}5p^0). The thermodynamic balance

between these two oxidation states is subtle, and both Sn(II) and Sn(IV) compounds are known to exist. SnS and SnS$_2$ are formed from a single oxidation state, while Sn$_2$S$_3$ is a multivalent compound, which can be described as Sn(II)Sn-(IV)S$_3$. The lower oxidation state is associated with a Sn lone pair,[26] which is the origin of the structural distortion found in the ground-state orthorhombic phase of SnS (Figure 1).[27]
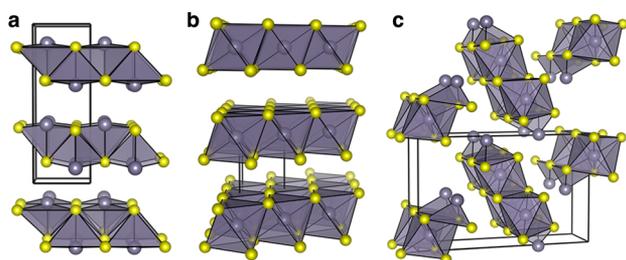
Figure 1. Ground-state crystal structures of the three phases of tin (gray) sulfide (yellow): (a) SnS, (b) SnS$_2$, and (c) Sn$_2$S$_3$.

In terms of conductivity, a reducible cation (i.e., tetravalent Sn) is generally associated with electron conduction (n-type), while an oxidizable cation (i.e., divalent Sn) is associated with hole conduction (p-type). Indeed, SnS$_2$ and Sn$_2$S$_3$ have been reported to be n-type semiconductors, whereas SnS exhibits p-type behavior.[28−31] It has been observed that a 15% deviation from ideal stoichiometry is sufficient to change the conduction of SnS from p- to n-type,[32] and it is thought that with appropriate control of the stoichiometry, a p−n junction can be formed from just tin and sulfur.[33,34] These factors re-enforce the hypothesis that deviations from ideal stoichiometry could be the cause of poor device performances recorded thus far.

There is confusion in the literature with respect to the assignment of distinct phases and the presence of alternate stoichiometries that cannot necessarily be discerned by common diffraction methods.[27,32,34] Indeed, as we will discuss, fundamental properties such as color, band gap, and the origin of free-carriers are still under debate and the current treatment of these materials is clearly not amenable to high performance applications. To understand the behavior of these materials in thin-films and nanoparticles, it is important to isolate the separate phases and to consider the distinct properties of each.[31]

We approach the problem by combining high-quality experiment and computation. The targeted synthesis of SnS, SnS$_2$, and Sn$_2$S$_3$ by chemical vapor transport (CVT) is used to produce macroscopic crystals, which have been characterized in terms of structure, morphology, and conductivity. The electronic structure and defect chemistry of the three materials have been modeled using density functional theory (DFT). Several inconsistencies are found with respect to phase-assignments and materials properties in the literature. Our results provide a platform to achieving sustainable light harvesting devices from Sn and S.

■ METHODS

Chemical Vapor Transport. Single crystals of tin sulfide have been grown previously by the Bridgman method[31] and chemical vapor transport,[35] and thin films formed by many different deposition methods.[24,32,36−42] CVT was first proposed by Schäfer as a way to vaporise metals at lower temperatures by forming a volatile chemical intermediate.[43] For tin, iodine has been shown as an optimum carrier

agent,[44] which has also been successfully applied to CZTS single crystals.[45]

The crystal growth apparatus consists of a horizontal tubular furnace (Elite Thermal Systems Ltd.) with four independently controlled zones within the furnace. The temperature components were chosen after calibration with a thermocouple drawn along inside of the furnace, such that the desired gradient was obtained across the length of the ampule (further details can be found in ref 45).

Tin (>99% powder, Aldrich) and stoichiometric amounts of sulfur (>99.999% pieces, Puratronic, hand crushed with an agate pestle and mortar) were placed in silica ampules that are 15 cm in length and 2 cm in diameter. Iodine (99.999% pieces, Aldrich) was placed in the same ampule, in quantities corresponding to the 5 mg cm^{-3} as recommended by Nitsche et al. to deliver the solid more slowly than the rate of crystal growth.[44] This ampule was then evacuated under the effect of liquid nitrogen in order to prevent the I$_2$ from evaporating under vacuum. Prior to ampule evacuation, all components were exposed to air and the associated content thereof, which represents a potential source of impurities, for example, oxidation or the inclusion of moisture. A schematic representation of the experimental system, and the chemical processes that this induces, is shown in Figure 2.

$$Sn + S + I_2 \quad \rightarrow \quad SnI_2 + S \quad \rightarrow \quad SnS + I_2$$
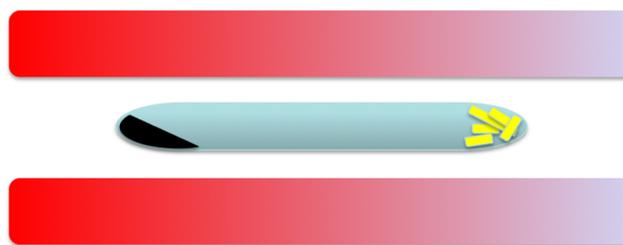
Figure 2. Schematic of the CVT process, with red showing higher and blue showing cooler temperatures. The crystals are in yellow and the solid components black. Tin migrates as tin iodide toward the cooler end of the ampule, where Sn−S stoichiometries form and release the iodine. I$_2$ diffuses back toward the tin to create a cycle.

Composition and Structural Characterization. The crystal structure for each of the phases was confirmed with X-ray Diffraction (XRD). Single-crystal XRD was performed on a Xcalibur, Atlas, Geminiultra X-ray diffractometer, for a Cu Kα radiation source. Powder-diffraction measurements were performed on a Bruker D8-Advance machine for a Cu Kα radiation source.

To assess the stoichiometries and morphology, a low-vacuum, high-performance JEOL-JSM-6610LV scanning electron microscope (SEM) fitted with an Oxford Instruments X-Max 800 mm energy-dispersive spectrometer (EDS) was used for multiple point-scans of the single crystals. The crystals were unpolished and unsputtered, but were washed with chloroform to remove any residual iodine from the CVT method.

Time-Resolved Microwave Conductivity. In pulse-radiolysis time-resolved microwave conductivity experiments (PR-TRMC), charges are generated in the sample by irradiation with high-energy electrons. The SnS, SnS$_2$, and Sn$_2$S$_3$ samples consisted of micrometer-sized crystallites that were diluted approximately ten times by mixing them with polymethylmethacrylate (PMMA) powder. To measure the conductivity, we inserted the sample into a microwave conductivity cell with the dimensions of a rectangular K$_a$ band microwave waveguide. The Sn$_x$S$_y$ samples were irradiated with nanosecond electron pulses of 3 MeV. The incident high-energy electrons undergo scattering within the sample and transfer energy by inducing ionisations. In this way a close to uniform distribution of positive charges (holes) and (secondary, ternary etc.) electrons is produced. The penetration depth of 3 MeV electrons is approximately 1.5 cm,

which exceeds the thickness of the microwave cavity (0.5 cm), hence, the incident 3 MeV electrons pass through the sample and charging does not occur. After the nanosecond electron pulse, the change in conductivity of the sample is probed as a function of time by monitoring the attenuation of reflected microwave power (frequency range between 28 and 38 GHz, maximum electric field strength in the sample 10 V/m). The fractional change in microwave power reflected by the cell ($\Delta P/P$) is directly proportional to the change in conductivity, $\Delta \sigma$ by

$$\frac{\Delta P}{P} = A\Delta\sigma = Ae\sum_i \mu_i n_i \qquad (1)$$

in which A is the sensitivity factor, n is the concentration of charges, and μ their mobility. The initial value of n, can be deduced using dosimetry measurements combined with an approximation of the average energy required to generate one electron–hole pair. Knowledge of n allows quantification of μ. A more detailed description of the PR-TRMC method can be found elsewhere.[46,47]

Computational Methods. The bulk phases of SnS, SnS_2, and Sn_2S_3 were simulated using Kohn–Sham DFT[48,49] within the plane-wave project-augmented wave formalism as implemented in the Vienna ab initio simulation package (VASP).[50,51] Electron exchange and correlation were described with the semilocal generalized gradient approximation (GGA) within the functional of Perdew, Burke and Ernzerhof optimized for solids (PBEsol).[52] The shallow core 4d states of Sn were explicitly treated as valence electrons. A plane-wave basis set (400 eV kinetic energy cutoff) was employed with well converged k-point sampling. To provide a quantitative prediction of the band gaps, hybrid-DFT was employed, incorporating 25% screened Hartree–Fock exchange to produce the HSE06 functional.[53]

All calculations were performed in closed-shell configurations (restricted spin), with geometry relaxations undertaken using the Broyden–Fletcher–Goldfarb–Shanno algorithm and a force convergence criterion tolerance in all cases of at least 0.01 eV/Å.[54] The equilibrium crystal structures and thermochemical data at this level of theory have previously been reported with good agreement with available experiment.[27]

The formation enthalpy of intrinsic point defects, tin and sulfur vacancies, was calculated using the supercell approach within the FHI-AIMS package,[55] and a previously reported method.[27] Lattice expansions of $(2 \times 4 \times 4)$, $(4 \times 4 \times 2)$, and $(2 \times 4 \times 1)$ were used for SnS, SnS_2, and Sn_2S_3 respectively. k-point sampling of at least $2 \times 2 \times 2$ was performed, consistent with the lengths of the reciprocal lattice vectors. The defect formation energies were calculated with respect to the elemental standard states (Sn metal and solid S_8).

■ RESULTS

Thermodynamics of Sn–I Transport. To guide the synthesis of the Sn–S phases by iodide vapor transport and help understand the underlying growth processes, a thermodynamic model of the relevant reactions was calculated. The stability region for each compound was found by minimizing the sum of the chemical potentials of the possible species on each side of the chemical equations as a function of the temperature, as taken from the database of Knacke et al.[56] We refer to previous work for detailed derivation of the equilibrium temperature ranges of stability for the species involved (e.g., iodine in the form of either atomic I or I_2).[57] The following reactions are assumed to be taking place ($x, y, w \in \mathbb{N}$; $1 \leq x \leq 2$; $1 \leq y \leq 8$; $0 \leq w \leq 1$):

- $SnS(s) + (4/x - 2(1 - w)/x)\ I_x(g) + 1/y\ S_y(g) \rightarrow SnI_{2(w+1)}(g) + 2/yS_y(g)$
- $SnS_2(s) + 24/xI_x(g) \rightarrow 6SnI_{2(w+1)}(g) + 12/yS_y(g) + 6(2 + 2w)/xI_x(g)$
- $3Sn_2S_3(s) + 24/xI_x(g) + 3/yS_y(g) \rightarrow 6SnI_{2(w+1)}(g) + 12/yS_y(g) + 6(2 + 2w)/xI_x(g)$

The Gibbs free energies of reaction as a function of the temperature are shown for each process in Figure 3.
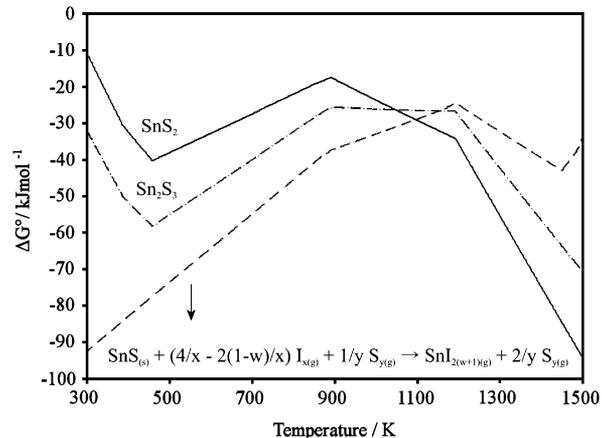
Figure 3. Standard Gibbs free energies of the reactions involved in the tin iodide formation for the vapor transport of SnS, Sn_2S_3, and SnS_2 as a function of the temperature.

Assuming thermodynamic equilibrium among the species in reactions 1–3 above, we can conclude that the equilibria involved in the transport of SnS, Sn_2S_3, and SnS_2 via tin iodide vapor are remarkably different. Therefore we foresee no thermodynamic hindrance to the effective separation of the crystallized phases given careful synthetic control.

Single-Crystal Growth. The CVT conditions required to synthesize SnS, SnS_2, and Sn_2S_3 are listed in Table 1, corresponding to the stoichiometric amounts of solid reagents.

Table 1. Reaction Conditions Used to Synthesize the Phases of Tin Sulfide Using CVT[a]

phase	temperature gradient (°C)	mass of tin (g)	mass of sulfur (g)	time (days)
SnS	850–950	1.579	0.427	10
SnS_2	600–850	1.691	0.897	12
Sn_2S_3	500–650	1.781	0.723	10

[a]In all reactions, approximately 250 mg of iodine was used as a carrier agent.

The reaction conditions agree well with the work of others,[35,44] but have the intriguing implication that in order to obtain phase pure SnS, rapid cooling may be necessary to escape the temperature window needed to synthesize Sn_2S_3 and/or SnS_2. Indeed rapid quenching of SnS below 650 °C was a practice observed by Lambros et al. in their isolation of "almost perfect" crystals.[58]

In our case, it was found that during the experiment for the synthesis of SnS_2, i.e., with highest sulfur load, both SnS_2 yellow flakes and Sn_2S_3 black needles were both obtained but were spatially separated within the ampule, with Sn_2S_3 being closer to the hotter side of the vessel compared to SnS_2. These findings are noteworthy because they agree with the thermochemical model derived in the previous section. The Gibbs free energy curves for the formation of tin iodide vapor from Sn_2S_3 and SnS_2 in Figure 3 show that the stability of SnS_2 against iodide formation is lower in the higher temperature side of the gradient applied, which is why this phase is expected to

444228222822

Table 2. Elemental Composition of Single Crystals Obtained As Atomic Percent Using Energy-Dispersive Spectroscopy and Their Macroscopic Appearance

Phase	S (%)	Sn (%)	Appearance	
SnS	50.46	49.54	dark grey amorphous solid	
SnS_2	68.42	31.58	yellow transparent flakes	
Sn_2S_3	60.12	39.88	shiny black needles	

Table 3. Reported Electron Transport Properties for the Tin Sulfides, Collected from Various Sources

phase	conductivity (Ω^{-1} cm^{-1})	carrier concentration (cm^{-3})	mobilities (cm^2 V^{-1} s^{-1})
SnS	0.077,[72] 0.069,[65] 0.05,[63] 0.033,[68] 0.030,[69] 6 × 10^{-5}, 5.3 × 10^{-5},[66] 4 × 10^{-5},[73]	1–3 × 10^{18} [15] 1.16 × 10^{17} [65] 1 × 10^{17},[74] 1.5 × 10^{16},[24] 1.2 × 10^{15},[72] 1 × 10^{15}, [68,69]	400–500,[72] 385,[74] 139,[69] 130,[68] 90,[15,67] 15.3,[24] 3.73[65]
SnS_2	0.90,[67] 1.3 × 10^{-2},[29] 2.4 × 10^{-5},[71] 3.9 × 10^{-7},[70]	2 × 10^{17},[67] 1 × 10^{13}, [71]	51.5,[67] 15[71]
Sn_2S_3	4.4 × 10^{-3},[30] 2.5 × 10^{-5}, [29]	9.42 × 10^{14}, [30]	"little information available"[67]

crystallize closer to the cold side of the reaction vessel. Conversely, the opposite argument can be applied for Sn_2S_3.

Stoichiometry and Structure Identification. The crystal structures of each material were confirmed using XRD. For Sn_2S_3 and SnS_2 single-crystal diffraction was possible, which confirmed the ground-state *Pnma* structure of Sn_2S_3 with structural parameters in agreement with previous reports.[59] For SnS_2 an extended $R\bar{3}$ polytype was identified, which is closely related to the known ground state $P\bar{3}m1$ phase but with an AAB layer stacking.[60] The ill-defined morphology of bulk SnS, resulting from the rapid cooling process from above its melting temperature, was not conducive to single-crystal diffraction; however, powder diffraction of a ground sample resulted in the expected *Pnma* phase.[61] To provide further evidence of the phase identities, we performed EDS analysis on our samples with results that are in agreement with the structural assignment (Table 2).

From XRD and EDS analysis, the phase assignment of the three materials is clear, with dark gray SnS, black needles of Sn_2S_3, and yellow flakes of SnS_2. However, this assignment is in contradiction to previous studies. Nitsche et al. reported their black needlelike crystals as SnS when following the same procedure we isolated Sn_2S_3.[44] Price et al. described yellow plates of Sn_2S_3 and black needles of SnS_2, the opposite of what we observe here.[62] Many more report on the tunability of SnS properties with different Sn:S ratio, when our results indicate that this is more likely to be a mechanical mixture of obtained phases rather than a homogeneous transition.[63,64]

Transport Properties. As previously discussed SnS is a natural p-type material with hole mediated transport. Reported conductivities range from 10^{-5} to 0.07 Ω^{-1} cm^{-1},[65,66] carrier concentrations from 10^{15} to 10^{18} cm^{-3}, and hole mobilities from 4 to 139 cm^2 V^{-1} s^{-1}.[65,67–69]

SnS_2 is an intrinsic n-type material. Reported conductivities range from 10^{-7} to 0.90 Ω^{-1} cm^{-1},[67,70] carrier concentrations from 10^{13} to 10^{17} cm^{-3}, and electron mobilities from 15 to 52 cm^2 V^{-1} s^{-1}.[67,71]

Sn_2S_3 has also been reported as an intrinsic n-type material with conductivities ranging from 10^{-5} to 10^{-3} Ω^{-1},[29,30] carrier concentrations around 10^{15} cm^{-3},[30] with no information available for charge carrier mobilities.[67]

All of these factors, listed in Table 3, will be crucial for optimization of the device applications of tin sulfide.

Microwave Conductivity. For photovoltaic applications, the charge carrier drift length is an important parameter, the value of which is given by the square root of the product of the lifetime of the light-induced charge carriers (τ) and their mobility (μ). To obtain these values for the tin sulfides, we performed pulse-radiolysis time-resolved microwave conductivity measurements.

Formation of mobile charges induces a rise in the electrical conductivity, which results in increased microwave absorption. The reduced amount of microwave power is detected on a nanosecond time scale as shown for SnS_2 and Sn_2S_3 in Figure 4. For SnS, the high dark conductivity of our crystals, i.e., the conductivity in absence of a pulse, does not allow microwave measurements using this setup.
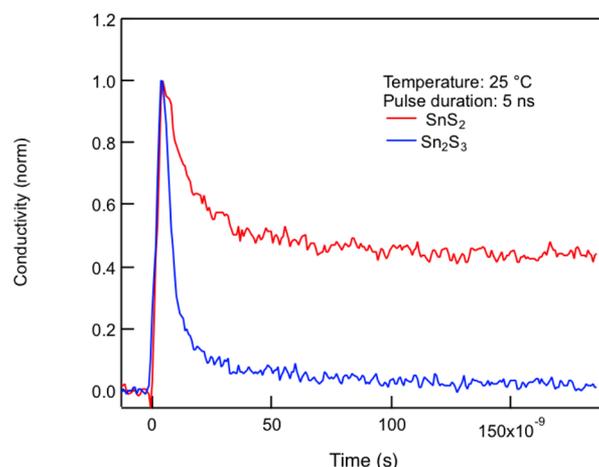
Figure 4. Normalized pulse radiolysis TRMC traces recorded for SnS_2 and Sn_2S_3 using a pulsed 3 MeV electron beam.

During the pulse, the signal rapidly increases because of the formation of mobile charge carriers (Fgure 4). The maximum signal size can be converted into a mobility using eq 1 as given in the experimental section, yielding for both materials a value of the order of 150 cm^2 V^{-1} s^{-1}. These are comparable to the highest values reported in the literature for these materials. Directly after the pulse, a fast decay is observable for both semiconductors; however, the decays are very different. The decay can be explained by the immobilization of charge carriers

due to, for example, electron trapping. Alternatively recombination of charge carriers also leads to a reduction in signal size. For Sn_2S_3, the signal decays to almost zero within a period of less than 50 ns. In contrast, the decay for SnS_2 is far slower and extends into the microsecond time scale.

The origin of the decay can be studied in more detail by changing the dose of the electron beam and comparing the dose normalized TRMC traces as shown in Figure 5. For SnS_2,
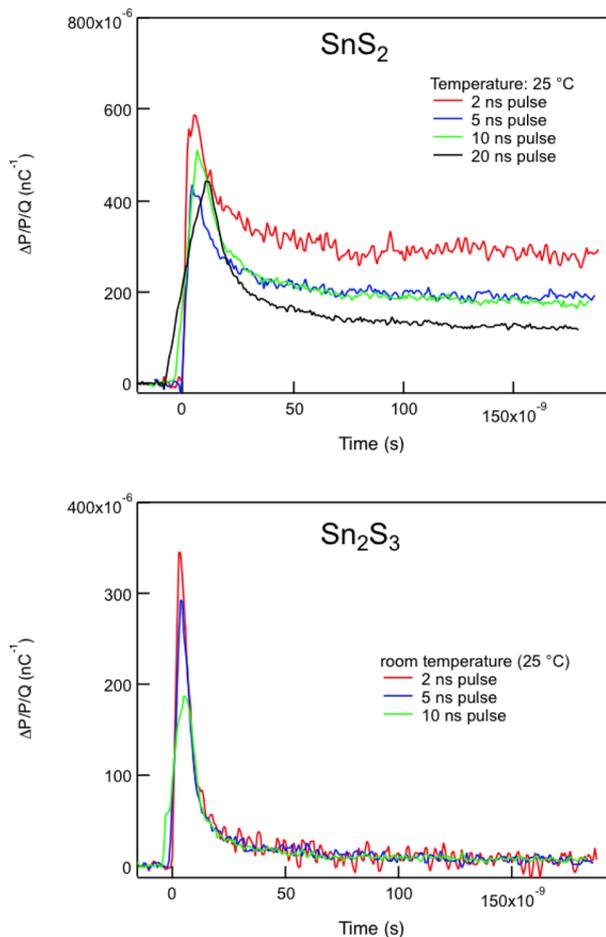
Figure 5. Dose-normalized change in conductivity for SnS_2 and Sn_2S_3. The x-axis shows time in nanoseconds and the y-axis shows the fractional change in microwave power reflected by the cell divided by the integrated beam charge per pulse (Q) in nano-Coulombs.

the signal decreases more rapidly as the dose increases. This is a clear sign of charge-carrier recombination according to second-order electron−hole kinetics. For Sn_2S_3, the decay is independent of the dose, indicating that trapping or recombination is a first-order process.

At the lowest pulse of 2 ns, for SnS_2, lifetime ($\tau_{1/2}$) is 50 ns and mobility (μ) is around 150 V^{-1} s^{-1}, giving a mobility lifetime product of 7.5×10^{-6} cm^2 V^{-1}. For Sn_2S_3, $\tau_{1/2} \approx 5$ ns and mobility is around 150 V^{-1} s^{-1}, giving a mobility lifetime product 7.5×10^{-7} cm^2 V^{-1}. These values are somewhat lower than those found for other materials, e.g., 7×10^{-5} cm^2 V^{-1} for CdTe.[75]

The signal for SnS_2 did decay to zero after a very long time (as shown in the Supporting Information). The long lifetimes can be attributed to the fact that the mobilities in different directions of the lattice vary by 4 orders of magnitude.[76] This large anisotropy in mobility is attributed to the two-dimen-

sional sheet like structures of the lattice in SnS_2 crystals. Interaction of the high energetic electrons of the accelerator pulse with the material induces the formation of charges over different sheets. Because the charge transport perpendicular to the sheets is slow, recombination of opposite charges is retarded.

The Einstein−Smoluchowski relation relates charge diffusion coefficient D to

$$D = \frac{\mu k_B T}{q} \tag{2}$$

where μ is mobility, k_B is the Boltzmann constant, T is temperature, and q is the electrical charge. Using the measured values of 150 cm^2 V^{-1} s^{-1} and 298 K for T, the charge diffusion coefficient is found to be 3.85 cm^2 s^{-1} for both samples.

For SnS, an important conclusion can be made from the absence of TRMC data. The promotion of electrons into higher energy states, necessary for the TRMC method, is also responsible for the splitting of the quasi Fermi levels, which dictates the open-circuit voltage in photovoltaic devices.[77] The background conductivity is a potential contributor to the poor V_{oc} observed to date.[17] As such, SnS devices might benefit from reducing the intrinsic conductivity through control of the growth conditions or extrinsic doping, as demonstrated with Sb recently.[25]

Defect Theory. To understand the microscopic origin of the conductivity in these undoped materials, we computed the energies associated with plausible defect reactions for each material at the DFT level of electronic structure methods. Defect concentrations were calculated following the law of mass action, under the assumption of thermal equilibrium at the growth temperature.[78] In SnS (SnS_2), a fully ionized tin vacancy would generate two (four) positive charge carriers (i.e., holes) and one sulfur vacancy would generate two negative charge carriers (i.e., electrons). These are expected to be the dominant native point defects.

As shown in Table 4, we corroborate the dependency of conductivity on defect stabilities and by extension predict typical charge carrier concentrations for each phase. The Sn vacancy has the lowest formation energy and highest concentration in SnS, which is consistent with that being the dominant acceptor defect. The S vacancy (in SnS) was thought to potentially act as an electron trap, but it has been shown that

Table 4. Point Defect Formation Energies and Concentrations Calculated under Sulfur-Rich Conditions (Atomic Exchange with a Reservoir of α-S) for the Neutral Defects at the Respective Synthesis Temperatures[a]

phase	space group	species	defect energy (eV)	concentration (cm^{-3})	type
SnS	Pnma	V_{Sn}	0.68	2.28×10^{19}	acceptor
	Pnma	V_S	2.17	6.57×10^{12}	
SnS_2	$P\bar{3}m1$	V_{Sn}	3.16	2.54×10^{04}	
	$P\bar{3}m1$	V_S	1.80	2.21×10^{12}	donor
Sn_2S_3	Pnma	$V_{Sn(1)}$	1.17	7.08×10^{14}	acceptor
	Pnma	$V_{Sn(2)}$	2.68	2.04×10^{05}	
	Pnma	$V_{S(1)}$	1.67	7.72×10^{11}	
	Pnma	$V_{S(2)}$	1.38	5.13×10^{13}	donor
	Pnma	$V_{S(3)}$	1.77	1.63×10^{11}	

[a]Multiple inequivalent sites for defect formation are distinguished with numerical subscripts. The dominant defects are indicated by their type.

the sulfur vacancies themselves do not compensate for the p-type contribution of tin vacancies (due to defect levels deep in the band gap).[23]

For SnS_2, the S vacancy dominates, which is consistent with its observed n-type behavior from charge balancing considerations . For Sn_2S_3, our results agree with observed behavior and go further to elucidate the intermediate behavior of Sn_2S_3, as a species containing both Sn(II) and Sn(IV) oxidation states. For SnS and SnS_2 the dominance of tin and sulfur vacancies, respectively, is unambiguous, which manifests as the observed longer carrier lifetimes and a second-order decay behavior for SnS_2. In Sn_2S_3, the formation energies of the two vacancy defects are very close in energy, which indicates that carrier concentrations should be sensitive to the growth or annealing conditions, and furthermore, the major carrier type might be subject to change. This prediction also explains the rapid recombination behavior shown in the previous section: the high concentration of donor sites can effectively compensate the n-type carriers and vice versa.

Electronic Structure. Because thin-film SnS samples typically show lower levels of conductivity than our crystals, we further explore the possibility that other phases could be present in "tin monosulfide" samples and films, corroborated by the persistent observation of "brown" films in literature and the wide variety of properties observed (see Tables 3 and 6).[79,80] Besides this, the fact that tin monosulfide and sesquisulfide have the same space group and similar XRD diffraction patterns means it is possible that the disappointing performance of SnS is due to an intrinsic alloy or mechanical mixture with Sn_2S_3. As mentioned in the introduction, it has been suggested that sulfur-rich conditions would be needed to avoid this occurrence, but such conditions alone were not sufficient to prevent off-stoichiometric phases of FeS_2 forming; another material that has so far failed to deliver as a PV absorber layer.[81]

The physical appearance of the single crystals suggests band gaps close to the IR region of the spectrum for SnS and Sn_2S_3 and a larger gap closer to the UV region for SnS_2 (i.e., yellow). Previous experimental measurements of the band gaps for each material are collected in Table 6. The values are wide-ranging:

Table 5. Calculated Fundamental Band Gaps of the Tin Sulfides Using the HSE06 Technique

phase	E_g (eV)
SnS	1.11 (indirect)
SnS_2	2.24 (indirect)
Sn_2S_3	1.09 (indirect)

1.08−1.70 eV for SnS, 1.82−2.41 eV for SnS_2, and 0.95−2.20 eV for Sn_2S_3. In addition to the form of materials, variation can also be attributed to fitting process, where the optical absorption spectrum is subject to a linear fit according to an idealized parabolic band dispersion. Of note are the number of fits to dipole forbidden transitions for fundamental band gaps.

Formally, these can occur only in centrosymmetric structures,[82] which does not correspond to any of the common tin sulfide phases. The results of our band structure calculations are included in Table 5. These are calculated at the experimental lattice constants to avoid any errors from the underlying structure.

Recent papers have reported calculated band gaps of SnS using G_0W_0 many-body perturbation theory based on local density approximation (LDA) structures or wave functions.[23,83] Our result of 1.11 eV would correspond to a room temperature band gap of 0.98 eV following the method outlined by Malone et al.[58,83] This value agrees well with the experimental observations of Zainal et al.[84]

The calculated valence band maxima, conduction band minima and vacuum potentials allow us construct a natural band offset diagram for each of the tin sulfide phases, which is shown in Figure 6. The procedure is detailed in ref 19, where
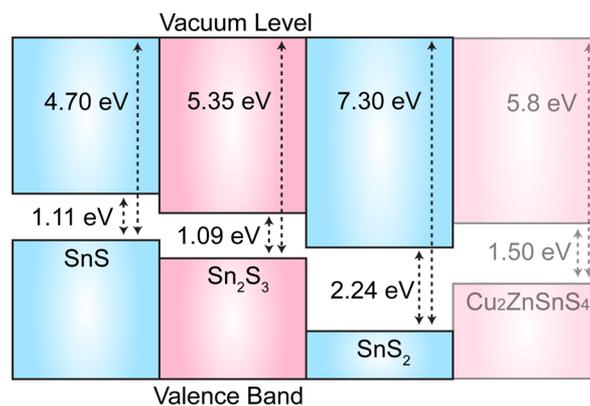
Figure 6. Calculated band offset diagram, using the HSE06 functional, for each of the three tin sulfide phases using a vacuum alignment procedure and that of CZTS for reference.[92]

electrostatic alignment is performed using the nonpolar (100) surface of SnS, a reconstructed (001) surface of Sn_2S_3, and a reconstructed (001) surface of SnS_2.

The lowest ionization potential is found for SnS (Figure 6), with a monotonic increase from Sn_2S_3 to SnS_2. Similarly, the electron affinity increases from 3.59 eV for SnS, to 4.24 eV for SnS_2, and 5.02 eV for Sn_2S_3. The calculations predict that the SnS/Sn_2S_3 and Sn_2S_3/SnS_2 interfaces would form p−n junctions of Type II nature, driving the separation of electrons and holes. However, the alignment between SnS and SnS_2 is of Type IIb, i.e., spontaneous electron and hole transfer would occur toward SnS.[93] With respect to SnS solar cells, a dispersion of these secondary phases (reported by multiple authors)[42,62,94−96] could decrease the open circuit voltage by mitigating the desired rectifying behavior across the cell. This could explain the limiting properties seen in devices as small-scale secondary phases and point defects have shown to be of macroscopic importance for Cu_2ZnSnS_4 (CZTS) cells.[97] Also

Table 6. Reported Optical Band Gaps of the Tin Sulfides from Thin-Film and Single Crystal Samples[a]

phase	reported optical E_g (eV)
SnS	0.9 −1.1 (indirect);[84] 1.08 (indirect);[15] 1.27 (allowed indirect);[85] 1.32 (direct),[65,69] 1.43 (direct);[41] 1.70 (direct);[34,66] 1.79 (direct)[86]
SnS_2	1.82 (forbidden indirect);[70] 2.07 (indirect);[87] 2.2 (forbidden indirect);[29] 2.41 (no further details)[88]
Sn_2S_3	0.95 eV (forbidden direct);[89] 1.05 (forbidden direct);[29] 1.16 (forbidden direct);[90] 1.6−1.9[79] 2 (direct);[30] 2.2 (indirect)[91]

[a]The type of band gap used in the fitting process is shown in parentheses.

of importance is the relatively low ionization potential of SnS compared to other photo absorbers (e.g., CZTS), which suggests that commonly used contacts such as molybdenum might not allow the effective separation of charges necessary for PV performance. The importance of appropriate contacts for SnS based solar cells has recently been highlighted.[19]

DISCUSSION AND CONCLUSIONS

Detailed examination of the tin sulfides has shown that the intrinsic material properties of the individual phases do not pose any insurmountable obstacles to the realization of their potential in respective photovoltaic or photochemical applications. Our characterization leads to the conclusion that the three stoichiometries of tin sulfide have been isolated and the identification of suitable methods allows for bulk production of phase-pure crystals.

Results obtained for SnS could provide an explanation as to the absence of high-efficiency PV devices with SnS as an absorber layer. Usually, the reported short circuit current is acceptable, yet the open circuit voltage is low. Indeed, due to a high background conductivity, the splitting of the quasi Fermi level will be difficult under illumination, and this will contribute to a low V_{oc} (typically lower than 200 mV). Careful control of the Sn:S stoichiometry is required to ensure that the concentration of Sn vacancies is sufficiently low; however, experimentally a low Sn content could also correspond to the formation of the alternative S-rich phases.

Our results for SnS_2 confirm that this material could be a good n-type buffer layer in thin-film solar cells, and could be quite thick, as the drift length of the electron carriers is sufficiently long. However, SnS_2 would form a metallic type IIb heterojunction with SnS that would be detrimental to a SnS/SnS_2 photovoltaic device as no depletion layer would form, although this may be overcome by tuning the morphology (e.g., dipoles) at the interface.

Finally, for Sn_2S_3, we confirm that it does not suffer from the same behavior as SnS (i.e., no large density of carriers in the dark), yet its carrier mobility is high (larger than amorphous silicon for example),[98] and its band gap is also attractive, more so than, for example, FeS_2.[99] The nature of Sn_2S_3 means that its presence in SnS films would inhibit transport physics, as a Type II junction would form between the two; similarly, any SnS present in an Sn_2S_3 sample would act as a hole trap and also limit performance. Because of the similarity in structural and vibrational (Raman/IR) properties of the various phases of tin sulfide, in order to assign the presence of Sn(II) and Sn(IV) in thin-film samples, characterization tools such as XPS and EXAFS could play an important role in the future.

In conclusion, we have synthesized single crystals of SnS, Sn_2S_3, and SnS_2 and investigated their electronic structure. The different semiconducting behavior of each phase can be explained from the underlying defect chemistry: p-type SnS (low energy Sn vacancies), n-type SnS_2 (low-energy S vacancies), and mixed-type Sn_2S_3 (accessible Sn and S vacancies). On the basis of analysis of the valence band alignments, we show that if phase pure samples are not obtained, and either of the other two known phases are present, then these would also be detrimental to transport properties and subsequently lower the photovoltaic device performance.

ASSOCIATED CONTENT

Ⓢ Supporting Information

Full X-ray crystallographic data for the three phases discussed in this paper and additional TRMC results for SnS_2. This material is available free of charge via the Internet at http://pubs.acs.org/.

AUTHOR INFORMATION

Corresponding Author

*E-mail: a.walsh@bath.ac.uk.

Notes

The authors declare no competing financial interest.

ACKNOWLEDGMENTS

REFERENCES

(1) Wadia, C.; Alivisatos, A. P.; Kammen, D. M. *Energy Environ. Sci.* **2009**, *43*, 2072−2077.

(2) Peter, L. M. *Philos. Trans. R. Soc. London, Ser. A* **2011**, *369*, 1840−1856.

(3) Scragg, J. J.; Dale, P. J.; Peter, L. M.; Zoppi, G.; Forbes, I. *Physica Status Solidi (b)* **2008**, *245*, 1772−1778.

(4) Chen, S.; Gong, X. G.; Walsh, A.; Wei, S. H. *Appl. Phys. Lett.* **2010**, *96*, 021902−3.

(5) Reddy, K. R.; Reddy, N. K.; Miles, R. *Sol. Energy Mater. Sol. Cells* **2006**, *90*, 3041−3046.

(6) Ferekides, C. S.; Balasubramanian, U.; Mamazza, R.; Viswanathan, V.; Zhao, H.; Morel, D. L. *Sol. Energy* **2004**, *77*, 823−830.

(7) Abou-Helal, M.; Boshta, M. *J. Am. Sci.* **2012**, *8*, 61−63.

(8) Reddy, K. R.; Reddy, P. P.; Datta, P.; Miles, R. *Thin Solid Films* **2002**, *403−404*, 116−119.

(9) Parenteau, M.; Carlone, C. *Phys. Rev. B* **1990**, *41*, 5227−5234.

(10) Anderson, J. S.; Morton, C. M. *Proc. Russ. Soc. A* **1945**, *184*, 873.

(11) Shockley, W.; Queisser, H. J. *J. Appl. Phys.* **1961**, *32*, 510−520.

(12) Nair, M. T. S.; Nair, P. K. *Semicond. Sci. Technol.* **1991**, *6*, 132.

(13) Prince, M. B. *J. Appl. Phys.* **1955**, *26*, 534−540.

(14) Loferski, J. J. *J. Appl. Phys.* **1956**, *27*, 777−784.

(15) Albers, W.; Haas, C.; J. Vink, H.; Wasscher, J. D. *J. Appl. Phys.* **1961**, *32*, 2220.

(16) Fthenakis, V. *Renew. Sust. Energy Rev.* **2009**, *13*, 2746−2750.

(17) Sinsermsuksakul, P.; Hartman, K.; Kim, S. B.; Heo, J.; Sun, L.; Park, H. H.; Chakraborty, R.; Buonassisi, T.; Gordon, R. G. *Appl. Phys. Lett.* **2013**, *102*, 053901.

(18) Reddy, N.; Reddy, K. T. R. *Conference Record of the Twenty Sixth IEEE Photovoltaic Specialists Conference*; Anaheim, CA, Sept 29−Oct 3, 2007 IEEE: Piscataway, NJ, 1997.

(19) Burton, L. A.; Walsh, A. *Appl. Phys. Lett.* **2013**, *102*, 132111.

(20) Scragg, J. J.; Watjen, J. T.; Edoff, M.; Ericson, T.; Kubart, T.; Platzer-Bjorkman, C. *J. Am. Chem. Soc.* **2012**, *134*, 19330−19333.

(21) Richard, A. P. Single Crystal Growth, Powder Synthesis and Characterization of Layered Chalcogenide Semiconductors. *Ph.D. thesis*, Oregon State University, Corvallis, OR, 2011.

(22) Reddy, K. R.; Reddy, P. P.; Miles, R.; Datta, P. *Opt. Mater.* **2001**, *17*, 295−298.

(23) Vidal, J.; Lany, S.; d'Avezac, M.; Zunger, A.; Zakutayev, A.; Francis, J.; Tate, J. *Appl. Phys. Lett.* **2012**, *100*, 032104.

(24) Sinsermsuksakul, P.; Heo, J.; Noh, W.; Hock, A. S.; Gordon, R. G. *Adv. Energy Mater.* **2011**, 1116−1125.

(25) Sinsermsuksakul, P.; Chakraborty, R.; Kim, S. B.; Heald, S. M.; Buonassisi, T.; Gordon, R. G. *Chem. Mater.* **2012**, *24*, 4556.

(26) Walsh, A.; Woodley, S. M. *Phys. Chem. Chem. Phys.* **2010**, *12*.

(27) Burton, L. A.; Walsh, A. *J. Phys. Chem. C* **2012**, *116*, 24262−24267.

(28) P. Boudjouk, S. R. B.; Seidler, D. J.; McCarthey, G. J. *Chem. Mater.* **1994**, *6*, 2108.

(29) Sanchez-Juarez, A.; Ortiz, A. *Semicond. Sci. Technol.* **2002**, *17*, 931.

(30) Khadraoui, M.; Benramdane, N.; Mathieu, C.; Bouzidi, A.; Miloua, R.; Kebbab, Z.; Sahraoui, K.; Desfeux, R. *Solid State Commun.* **2010**, *150*, 297−300.

(31) Nassary, M. *J. Alloys Compd.* **2005**, *398*, 21−25.

(32) Huang, C.-C.; Lin, Y.-J.; Chuang, C.-Y.; Liu, C.-J.; Yang, Y.-W. *J. Alloys Compd.* **2013**, *553*, 208−211.

(33) Sanchez-Juarez, A.; Tiburcio-Silver, A.; Ortiz, A. *Thin Solid Films* **2005**, *480?481*, 452−456.

(34) Ogah, O. E.; Zoppi, G.; Forbes, I.; Miles, R. *Thin Solid Films* **2009**, *517*, 2485−2488.

(35) Cruz, M.; Morales, J.; Espinos, J. P.; Sanz, J. *J. Solid State Chem.* **2003**, *175*, 359−365.

(36) Kana, A. T.; Hibbert, T. G.; Mahon, M. F.; Molloy, K. C.; Parkin, I. P.; Price, L. S. *Polyhedron* **2001**, *20*, 2989−2995.

(37) Nair, P. K.; Nair, M. T. S.; Garcia, V. M.; Arenas, O. L.; Pena, Y.; Castillo, A.; Ayala, I. T.; Gomezdaza, O.; Sanchez, A.; Campos, J.; Hu, H.; Suarez, R.; Rincon, M. E. *Sol. Energy Mater. Sol. Cells* **1998**, *52*, 313−344.

(38) Ghazali, A.; Zainal, Z.; Hussein, M. Z.; Kassim, A. *Sol. Energy Mater. Sol. Cells* **1998**, *55*, 237−249.

(39) Sugiyama, M.; Miyauchi, K.; Minemura, T.; Ohtsuka, K.; Noguchi, K.; Nakanishi, H. *Jpn. J. Appl. Phys.* **2008**, *47*, 4494−4495.

(40) Xu, Z.; Chen, Y. *Semicond. Sci. Technol.* **2012**, *27*, 035007.

(41) Ghosh, B.; Das, M.; Banerjee, P.; Das, S. *Appl. Surf. Sci.* **2008**, *254*, 6436−6440.

(42) Hartman, K.; Johnson, J.; Bertoni, M. I.; Recht, D.; Aziz, M. J.; Scarpulla, M. A.; Buonassisi, T. *Thin Solid Films* **2011**, *519*, 7421−7424.

(43) Schafer, H. *Z. Anorg. Chem* **1956**, *286*, 42.

(44) Nitsche, R.; Bolsterli, H. U.; Lichtensteiger, M. *J. Phys. Chem. Solids* **1961**, *21*, 199−205.

(45) Colombara, D.; Delsante, S.; Borzone, G.; Mitchels, J.; Molloy, K.; Thomas, L.; Mendis, B.; Cummings, C.; Marken, F.; Peter, L. *J. Cryst. Growth* **2013**, *364*, 101−110.

(46) Schouten, P. G.; Warman, J. M.; de Haas, M. P. *J. Phys. Chem.* **1993**, *97*, 9863−9870.

(47) Warman, J. M.; de Haas, M. P.; Dicker, G.; Grozema, F. C.; Piris, J.; Debije, M. G. *Chem. Mater.* **2004**, *16*, 4600−4609.

(48) Hohenberg, P.; Kohn, W. *Phys. Rev.* **1964**, *136*, B864−B871.

(49) Kohn, W.; Sham, L. J. *Phys. Rev.* **1965**, *140*, A1133−A1138.

(50) Kresse, G.; Furthmüller, J. *Phys. Rev. B* **1996**, *54*, 11169.

(51) Kresse, G.; Joubert, D. *Phys. Rev. B* **1999**, *59*, 1758.

(52) Perdew, J. P.; Ruzsinszky, A.; Csonka, G. I.; Vydrov, O. A.; Scuseria, G. E.; Constantin, L. A.; Zhou, X.; Burke, K. *Phys. Rev. Lett.* **2008**, *100*, 136406.

(53) Heyd, J.; Scuseria, G. E.; Ernzerhof, M. *J. Chem. Phys.* **2006**, *124*, 219906.

(54) Head, J. D.; Zerner, M. C. *Chem. Phys. Lett.* **1985**, *122*, 264−270.

(55) Blum, V.; Gehrke, R.; Hanke, F.; Havu, P.; Havu, V.; Ren, X.; Reuter, K.; Scheffler, M. *Comput. Phys. Commun.* **2009**, *180*, 2175−2196.

(56) Knacke, O.; Kubaschewski, O. *Thermochemical Properties of Inorganic Substances*, 2nd ed.; Springer-Verlag: Dusseldorf, Germany, 1991.

(57) Colombara, D. Investigation of Chalcogenide Absorber Materials for Photovoltaic Applications. *Ph.D. thesis,* University of Bath, Bath, U.K., 2012.

(58) Lambros, A.; Geraleas, D.; Economou, N. *J. Phys. Chem. Solids* **1974**, *35*, 537−541.

(59) Kniep, R.; Mootz, D.; Severin, U.; Wunderlich, H. *Acta Crystallogr., Sect. B* **1982**, *38*, 2022−2023.

(60) Hazen, M. R.; Finger, L. W. *Am. Mineral.* **1978**, *63*, 289−292.

(61) Chattopadhyay, T.; Pannetier, J.; Von Schnering, H. G. *J. Phys. Chem. Solids* **1986**, *47*, 879−885.

(62) Price, L. S.; Parkin, I. P.; Hardy, A. M. E.; Clark, R. J. H.; Hibbert, T. G.; Molloy, K. C. *Chem. Mater.* **1999**, *11*, 1792−1799.

(63) Guang-Pu, W.; Zhi-Lin, Z.; Wei-Ming, Z.; Xiang-Hong, G.; Wei-Qun, C.; Tanamura, H.; Yamaguchi, M.; Noguchi, H.; Nagatomo, T.; Omoto, O. *Photovoltaic Energy Conversion, 1994, Conference Record of the Twenty Fourth IEEE Photovoltaic Specialists Conference*; Waikoloa, HI, Dec 5−9, 1994 ; IEEE: Piscataway, NJ, 1994.

(64) Ristova, M.; Ristov, M. *Sol. Energ. Mat. Sol. C.* **1998**, *53*, 95−102.

(65) Yanuar; Guastavino, F.; Llinares, C.; Djessas, K.; Masse, G. *J. Mater. Sci. Lett.* **2000**, *19*, 2135−2137.

(66) Calixto-Rodriguez, M.; Martinez, H.; Sanchez-Juarez, A.; Campos-Alvarez, J.; Tiburcio-Silver, A.; Calixto, M. *Thin Solid Films* **2009**, *517*, 2497−2499.

(67) Madelung, O. *Semiconductors: Data Handbook*, 3rd ed.; Springer: New York, 2004.

(68) Reddy, N. K.; Reddy, K. R. *Solid-State Electron.* **2005**, *49*, 902−906.

(69) Reddy, N. K.; Reddy, K. T. R. *Mater. Chem. Phys.* **2007**, *102*, 13−18.

(70) Amalraj, L.; Sanjeeviraja, C.; Jayachandran, M. *J. Cryst. Growth* **2002**, *234*, 683−689.

(71) Julien, C.; Eddrief, M.; Samaras, I.; Balkanski, M. *Mater. Sci. Eng., B* **1992**, *15*, 70−72.

(72) Noguchi, H.; Setiyadi, A.; Tanamura, H.; Nagatomo, T.; Omoto, O. *Sol. Energy Mater. Sol. Cells* **1994**, *35*, 325−331.

(73) Nair, M. T. S.; Nair, P. K. *Semicond. Sci. Technol.* **1991**, *6*, 132.

(74) Wangperawong, A.; Herron, S. M.; Runser, R. R.; Hägglund, C.; Tanskanen, J. T.; Lee, H.-B.-R.; Clemens, B. M.; Bent, S. F. *Appl. Phys. Lett.* **2013**, *103*, No. 052105.

(75) Sellin, P.; Davies, A. W.; Lohstroh, A.; Ozsan, M.; Parkin, J. *IEEE Trans. Nucl. Sci.* **2005**, *52*, 3074−3078.

(76) Patil, R. H.; Tredgold, S G *J. Phys. D: Appl. Phys.* **1971**, *4*, 718−722.

(77) Markvart, T. *Prog. Quant. Electron.* **2000**, *24*, 107−186.

(78) de Walle, C. G. V.; Neugebauer, J. *J. Appl. Phys.* **2004**, *95*, 3851−3879.

(79) Engelken, R. D.; McCloud, H. E.; Lee, C.; Slayton, M.; Ghoreishi, H. *J. Electrochem. Soc.* **1987**, *134*, 2696−2707.

(80) Cheng, S.; Zhang, H. *Micro Nano Lett.* **2011**, *6*, 473−475.

(81) Yu, L.; Lany, S.; Kykyneshi, R.; Jieratum, V.; Ravichandran, R.; Pelatt, B.; Altschul, E.; Platt, H. A. S.; Wager, J. F.; Keszler, D. A.; Zunger, A. *Adv. Energy Mater.* **2011**, *1*, 748−753.

(82) Atkins, P.; Overton, T.; Rourke, J.; Weller, M.; Armstrong, F. *Inorganic Chemistry*; Oxford University Press: Oxford, U.K., 2006.

(83) Malone, B. D.; Kaxiras, E. *Phys. Rev. B* **2013**, *87*, 245312.

(84) Zainal, Z.; Hussein, M. Z.; Ghazali, A. *Sol. Energy Mater. Sol. Cells* **1996**, *40*, 347−357.

(85) Lopez, S.; Ortiz, A. *Semicond. Sci. Technol.* **1994**, *9*, 2130−2133.

(86) Ragina, A. J.; Murali, K. V.; Preetha, K. C.; Deepa, K.; Remadevi, T. L. A Study of Optical Parameters of Tin Sulphide Thin Films Using the Swanepoel Method. *Optics: Phenomena, Materials, Devices, and Characterization 2011: International Conference on Light* ; Calicut, India,

Chemistry of Materials

May 23−25, 2011 ; American Institute of Physics: College Park, MD, 2011

(87) Domingo, G.; Itoga, R. S.; Kannewurf, C. R. *Phys. Rev.* **1966**, *143*, 536−541.

(88) Shi, C.; Chen, Z.; Shi, G.; Sun, R.; Zhan, X.; Shen, X. *Thin Solid Films* **2012**, *520*, 4898−4901.

(89) Alpen, U.; Fenner, J.; Gmelin, E. *Mater. Res. Bull.* **1975**, *10*, 175−180.

(90) Lopez, S.; Granados, S.; Ortiz, A. *Semicond. Sci. Technol.* **1996**, *11*, 433.

(91) Salah, H. B. H.; Bouzouita, H.; Rezig, B. *Thin Solid Films* **2005**, *480?481*, 439−442.

(92) Walsh, A.; Chen, S.; Wei, S.-H.; Gong, X.-G. *Adv. Energy Mater.* **2012**, *2*, 400−409.

(93) Yu, P. Y.; Cardona, M. *Fundamentals of Semiconductors*, 3rd ed.; Springer-Verlag: New York, 2003.

(94) Mathews, N. R.; Anaya, H. B. M.; Cortes-Jacome, M. A.; Angeles-Chavez, C.; Toledo-Antonio, J. A. *J. Electrochem. Soc.* **2010**, *157*, H337−H341.

(95) Miles, R. W.; Ogah, O. E.; Zoppi, G.; Forbes, I. *Thin Solid Films* **2009**, *517*, 4702−4705.

(96) Barone, G.; Hibbert, T. G.; Mahon, M. F.; Molloy, K. C.; Price, L. S.; Parkin, I. P.; Hardy, A. M. E.; Field, M. N. *J. Mater. Chem.* **2001**, *11*, 464−468.

(97) Scragg, J. J.; Kubart, T.; Watjen, J. T.; Ericson, T.; Linnarsson, M. K.; Platzer-Bjorkman, C. *Chem. Mater.* **2013**, *25*, 3162−3171.

(98) Moore, A. R. *Appl. Phys. Lett.* **1977**, *31*, 762−764.

(99) *Handbook of Optical Constants of Solids*, 3rd ed.; Academic Press: London, 1998.

(100) Momma, K.; Izumi, F. *J. Appl. Crystallogr.* **2011**, *44*, 1272−1276.